A Theoretical Study of Cu(II) Sites in a Faujasite-Type Zeolite: Structures and Electron Paramagnetic Resonance Hyperfine Coupling Constants

Dorothée Berthomieu,* Jean-Marie Ducéré, and Annick Goursot

Laboratoire de Matériaux Catalytiques et Catalyse en Chimie Organique, UMR CNRS-5618, ENSCM, 8 rue de l'Ecole Normale, 34296 Montpellier Cedex 5, France

Received: December 31, 2001; In Final Form: May 16, 2002

Calculations using a density functional theory-based methodology have been performed to study the electron paramagnetic resonance (EPR) properties of Cu(II)−faujasite models. Cluster models of sites II and III have been investigated. The calculated spin density is distributed both on Cu and on the framework atoms. Its value for Cu depends on its local bonding interactions with the zeolite framework. The calculated hyperfine coupling constants vary linearly with the calculated Cu spin density, whatever the models and methodologies are. Comparison with experimental results shows that Cu cations in four- and six-membered rings (sites III and II) can be related with the measured EPR signals, although no explicit site−signal correlation could be found.

I. Introduction

Copper(II)-exchanged zeolites are powerful and useful catalysts. In particular, they present a very high catalytic activity for the decomposition of NO and are thus involved in the depollution of the effluents of gas as well as in the selective catalytic reduction (SCR) process using NH_3.[1−3] Zeolites are materials containing cages and (or) channels resulting from arrangements of SiO_4 and AlO_4 tetrahedra bonded by edges and corners. The negative charges generated by Al substitutions are compensated by cations, which occupy some of the crystallographic positions. Most generally, copper(II) zeolites are obtained by exchange of alkali cations. Different experimental approaches, like magnetic resonance and X-ray spectroscopies, are used to get information on the structure of the solids including the positions of the extraframework cations. However, the X-ray techniques cannot distinguish Si and Al, leading then to average values for the Si−O/Al−O bond lengths and to an artificially higher symmetry group. There is thus no available information about the Cu sites.

Electron paramagnetic resonance (EPR) is a powerful and very adequate technique giving a fingerprint of paramagnetic cations in zeolites. However, the interpretation of the EPR spectra reported for Cu(II)−Y zeolites is not trivial and the locations of Cu(II) cations are still subject to debate. The architecture of the Y zeolite contains cages resulting from the arrangement of four- and six-membered rings of SiO_4/AlO_4 tetrahedra. The compensating cations are located at different positions in those cages, that is, sites I/I′, II/II′, and III (Figure 1). Experimental EPR spectra of Cu−Y zeolites display several signals, which have been generally attributed to Cu at sites I/I′ and II/II′.[4−9] Moreover, electron spin−echo studies of the fine interaction of Al nuclei with copper[10,11] have shown that the presence of Al in the Cu neighborhood influences the g tensor values: $g_{\|}$ is higher when Cu is centered in the plane containing the Al nuclei than when it is slightly on top. These results have suggested a recent theoretical study[12] in which the authors have shown that Cu(II) located at site II with different Si/Al ratios (Si/Al = 5, 2, 1) and different Al distributions corresponds to different g values, which fit with their two observed signals.

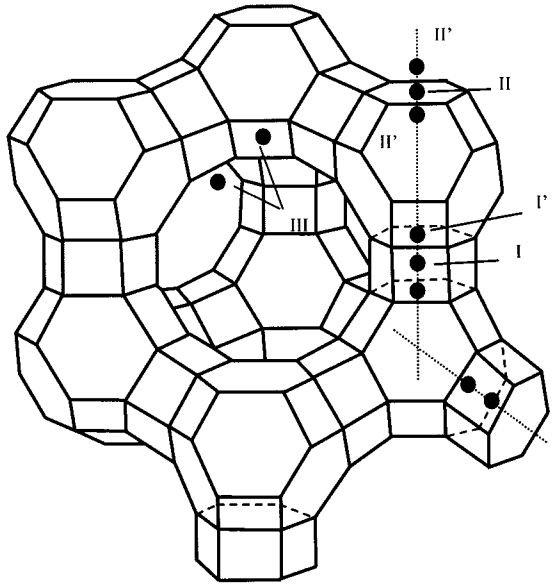

Figure 1. Faujasite-type structure with cationic sites.

These results illustrate that the interpretation of experimental EPR spectra is very delicate, even when considering only site II for the Cu position. In fact, the problem is certainly more complicated because X-ray studies have also found Cu(II) at sites III.[13] Finally, it is well-known that the positions of Cu(II) in zeolite Y can be controlled by the presence of cocations, that is, alkali cations with some of which Cu cations have been exchanged.[14,15] For example, in the SCR of NO with NH_3, it has been shown that the presence of barium or lanthanide cations, mostly located at sites I/I′, enhances the activity of the catalyst and that also the reaction becomes fully selective. This result has been attributed to an increased accessibility of Cu in the supercages (sites II and III). Furthermore, the EPR spectra of catalysts containing Ba^{2+} as cocations include two signals

* To whom correspondence should be addressed. E-mail: bertho@univ-montp2.fr.

10.1021/jp014698u CCC: $22.00
Published on Web 07/03/2002

instead of three signals in the presence of Na^+, indicating that one less position is available for copper when the cocation is Ba^{2+}.[6,16]

In this study, we have investigated the possible locations of Cu(II) cations at sites II and III of a Y zeolite (Figure 1) and compared the calculated EPR parameters obtained with model clusters to experimental values. We have focused our interest on the study of the hyperfine properties of these models, and most particularly on the anisotropic coupling, to verify whether we can provide a valuable help for the interpretation of the experimental EPR spectra. Finally, we will show that this comparison with experiment allows us to propose a "molecular" description of the transition metal cation−zeolite interactions.

II. Computational Details

II-1. Methods. These calculations have been performed using a density functional theory (DFT)-based methodology with the deMon-KS[17] and Gaussian 98[18] programs. Graphical geometry representations have been performed using MOLEKEL.[19]

Calculations labeled m-BP correspond to a mixed scheme in which the density has been obtained at the local level (with a Vosko−Wilk−Nusair correlation potential)[20] and the energy calculated at the gradient-corrected (GGA)[21] level using Becke's corrections for exchange[22] and Perdew's corrections for correlation.[23] The full GGA calculations with nonlocal corrections for potential and energy, that is, Becke exchange[22] and Perdew correlation functionals [23] are labeled BP. We have also used the B3LYP hybrid methodology.[24,25]

We have used the Wachters basis set (without f orbitals) for copper,[26] a DZVP quality basis[27] for all other heavy atoms, and a DZ basis[27] for hydrogen atoms. In Huzinaga's notation, their contraction patterns are (6321/521/1*), (621/41/1*), and (41) for Si and Al, O, and H, respectively. The associated auxiliary basis sets used to fit the density and the exchange−correlation potential[27] are, with respect to the same atoms, (5,4;5,4), (5,2;5,2), and (5,1;5,1), where the usual deMon notation is used. We have also used the 6-31G(d) basis set[28,29] and the more-extented triple-ζ quality basis set 6-311+G(2d,2p)[30,31] and IGLOIII basis set[32] for Si, Al, O, and H for the BP and B3LYP calculations involved in the Gaussian 98 program.[18]

Geometry optimizations using DFT methods have been considered converged when energy changes were less than 10^{-5} hartree, and the SCF convergence criterion was 10^{-6} hartree. All of the EPR properties were calculated with the Gaussian 98 program to facilitate the comparison between the BP and B3LYP values because deMon has not been developed for hybrid calculations.

II-2. Hyperfine Coupling. In general, the experimental values of the $A_{||}$ and $A_{\perp}$ components of the hyperfine coupling can be obtained, although $A_{\perp}$ is often not detectable. In the case of axial symmetry, $A_{||} = (T_{zz} + A_0)$ and $A_{\perp} = [{}^1/_2(T_{xx} + T_{yy}) + A_0]$, where T and A_0 represent the anisotropic and isotropic (Fermi) couplings, respectively. In most cases, the A_0 value is not known experimentally. To get rid of this contribution, which, moreover, remains a challenge for theoretical calculations, we have made use of the variable $A_{dip} = {}^1/_3|A_{||} - A_{\perp}| = {}^1/_2 T_{zz}$[33] for the comparison of calculated and experimental results.

The anisotropic hyperfine coupling has been calculated at the first-order approximation, that is, without including the spin−orbit contributions. The components of this anisotropic tensor are calculated according to the following expression:[34]

$$T_{uv}(N) = g_e\beta_e g_N\beta_N \sum_{\mu\nu} P_{\mu\nu}^{\alpha-\beta} \langle \phi_\mu | r_{Ni}^{-5} (r_{Ni}^2 \delta_{uv} - 3 r_{Niu} r_{Niv}) | \phi_\nu \rangle$$

where r_{Ni} = the position of electron i with respect to nucleus N and r_{Niu} and r_{Niv} = the components of r_{Ni} in the x, y, and z reference axes. β_e, β_N, g_e, and g_N are the Bohr magneton, nuclear magneton, free electron, and nuclear g values, respectively. $P_{\mu\nu}^{\alpha-\beta}$ is the spin density matrix element related to orbitals ϕ_μ and ϕ_ν ($P_{\mu\nu}^{\alpha} - P_{\mu\nu}^{\beta}$ is the difference between the α and β density matrix elements).

Spin−orbit effects contribute to the hyperfine coupling constants A_0 and A_{dip} by second-order terms. When covalency is important, contribution of the ligands in the spin−orbit perturbation may not be negligible. A posteriori corrections can be applied for metal complexes of high symmetry.[33] They appear not to be easy for models without symmetry, large delocalization of the unpaired electron, and low-lying excited states.[35]

II-3. Models of Sites II and Sites III of Cu−Y: Geometries. Accurate theoretical geometries would necessitate taking into account the whole solid, which is not possible because of the large size of the faujasite unit cell and the unknown distribution of Al in the framework. To reproduce some trends of the real structure, we have chosen to use a cluster cut from a solid defined by X-ray parameters[13] with dangling bonds saturated with hydrogen atoms, which have been positioned along the corresponding O−Si or Si−O bond vectors in the original experimental structure. The resulting O−H bonds were set to 1.0 Å and the Si−H bonds to 1.5 Å. All models include two Al to keep the system neutral. Moreover, different Al topologies have been investigated with the restriction imposed by the Loewenstein's rule that two Al should be separated by at least one Si. The geometries of all of these clusters have been optimized keeping fixed the hydrogen atoms to reproduce the constraints of the solid. Because of this restriction, frequency calculations cannot be used to confirm that the optimized structures correspond to minima of the total energy. For an easier comparison of the different site II models, their terminal H atoms have been taken at the same positions.

Another way to obtain consistent starting geometries is to use structures provided by molecular mechanics (MM) optimization using periodic boundary conditions and a random distribution of Al for a Si/Al ratio of 2.5 (Cerius2,[36] cvff-aug-ionic force field). The MM optimization has been performed using Co^{2+} parameters for copper, because adequate Cu^{2+} Lennard-Jones parameters are missing. These approximate positions for Cu^{2+} have then been optimized quantum chemically (labeled QM/MM), the framework atoms being kept fixed at the MM solid geometry. These procedures have been adopted to take into account the long-range interactions between the cluster and its surroundings, in particular neighboring cations. The clusters the geometries of which have been obtained with these procedures are labeled using the MM and QM/MM superscript ($iCuY_{B'}^{QM/MM}$, $CuY_{F'}^{QM/MM}$, $CuY_{F'}^{MM}$). The clusters chosen to represent Cu(II) at sites III and II are presented in Figures 2 and 3, respectively.

The structures, reported in Figures 2 and 3, correspond to local energy minima, but they are certainly not the unique possible models for Cu sites in the supercage. Different structures and conformers have been investigated to analyze the evolution of the electronic properties as a function of the environment of copper. For site III (Figure 2), the cation has been considered in the supercage (CuY_A, CuY_B, $CuY_{B'}$, CuY_C, CuY_D, and $CuY_{D'}$), on top of a four-membered ring ($iCuY_B$, $iCuY_{B'}$) or on top of two four-membered rings (CuY_E). All structures correspond to a bicoordinated metal except $iCuY_B$, $iCuY_{B'}$, and CuY_E in which the cation is involved in four and

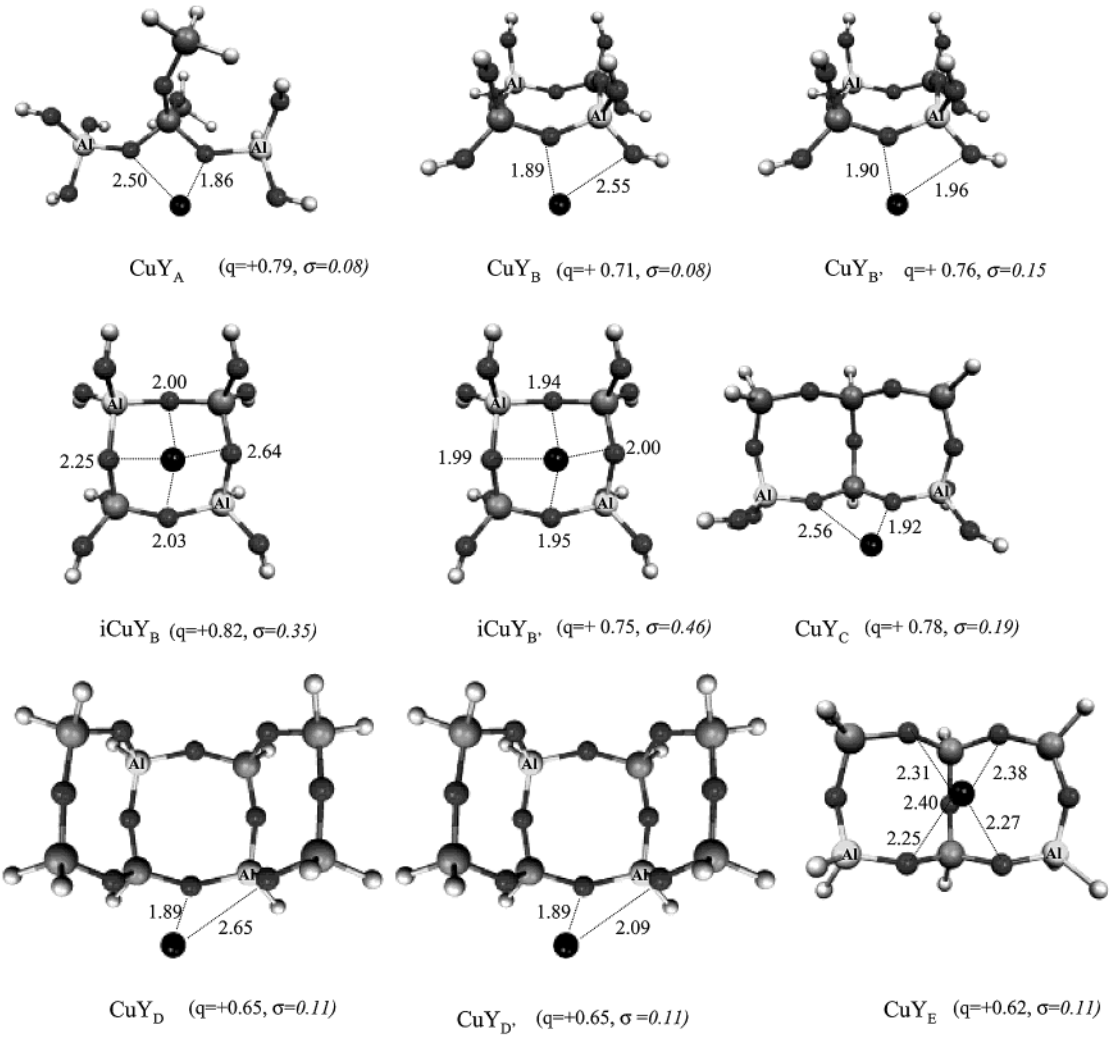

Figure 2. Different structures of site III models. Properties were calculated using the BP methods, together with Wachters basis set on copper, DZVP basis sets on heavy atoms, and a DZ basis set on H. The q and σ notations indicate the Mulliken net charge and spin density on copper, respectively. Cu is represented by black balls, H by small white balls, O by small dark balls, Si by gray balls, and Al by labeled balls.

five metal−zeolite oxygen bonds. In the case of bicoordinated Cu models, different cluster sizes and Al distributions have been considered.

When copper is bicoordinated to a single four-membered ring, two different isomers (CuY_B, $CuY_{B'}$) of comparable energies but with different Cu−O bond lengths have been found. In ideal position, the Cu(II) ion is located close to the center of the four-membered ring. In this case also, two conformers ($iCuY_B$, $iCuY_{B'}$) with different metal−oxygen distances have been localized: $iCuY_B$ contains three short and one longer Cu−O bonds, whereas the $iCuY_{B'}$ isomer corresponds to four short Cu−O bonds. The $iCuY_{B'}^{QM/MM}$ optimized structure is similar to $iCuY_{B'}$ with four equivalent but slightly longer Cu−O bonds (Table 1).

In contrast to site III, optimized site II geometries (Figure 3, Table 2) differ significantly from the corresponding X-ray structure. This is probably because there are more degrees of freedom inducing a higher flexibility of site II in comparison with four-membered ring systems. Whereas, in the literature, site II is usually considered as containing three short metal−oxygen bonds, our models with two Al display four Cu−O bonds.

Two isomers are possible for site II models: one containing the Al−Si−Al sequence (1,3 −2Al) and the other one the Al−Si−Si−Al sequence (1,4 −2Al). Although the probability to have the 1,3 −2Al isomers is higher for a random Al distribution, the first structure is less stable than the second one. This remark is however not determinant because the zeolite framework is grown with alkali cations (for example, K^+) for which the relative positions (Al, cations) and stabilities are certainly different. The 1,3 −2Al geometries (CuY_{F1} and $CuY_{F1'}$) are very comparable with those reported recently.[12] In these clusters, Cu(II) is not at the center of the ring, because the ring as no symmetry, but is closer to Al rather than Si, as it is generally observed experimentally.[37] The optimized models can be divided into two groups: one group contains four short Cu−O bonds, and the other one contains three short and one longer Cu−O bonds. The structures with four ring O−(Al) connected to Cu are more stable than those with only three O(Al)−Cu bonds. Shorter Cu−O bond lengths correspond to larger metal−zeolite interactions. In the QM/MM-optimized structure also, four ring O−(Al) are bonded to Cu. In that case, the resulting energy is higher than those with QM-optimized geometries because only the Cu position has been optimized. Whatever the methods used are, the deformation of the six-membered ring allows Cu(II) to reach a stable square-planar environment (the four ring O are quasi-coplanar with Cu(II)).

As already reported for site III,[38] the frontier orbitals of the site II models are distributed on copper and on the zeolite oxygen atoms. The SOMO stabilizes the system with an overlap

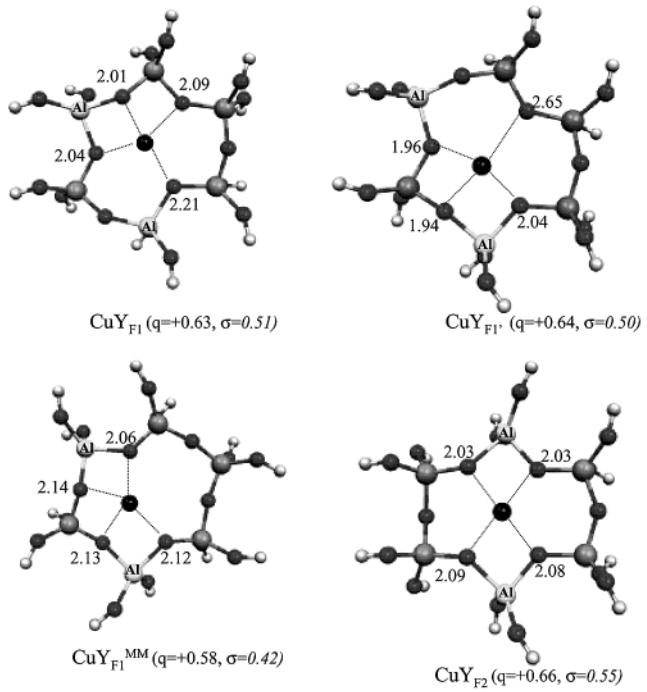

Figure 3. Different structures of site II models. Properties were calculated using the BP methods, together with Wachters basis set on copper, DZVP basis sets on heavy atoms, and a DZ basis set on H. The q and σ notations indicate the Mulliken net charge and spin density on copper, respectively. Cu is represented by black balls, H by small white balls, O by small dark balls, Si by gray balls, and Al by labeled balls.

TABLE 1: Site III Models, Cu−O Bond Lengths, Geometry Optimization Methods and Calculation Types, Mulliken Cu Net Charge, Spin Density, and A_{dip} Values (6-31G(d) for All Atoms and Wachters for Cu)

models[a]	geometry optimization method	d_{Cu-O} (Å)	calculation energy method	Mulliken metal net charge	spin density	A_{dip} (10^{-4} cm^{-1})
CuY_B	BP	1.89	BP	0.51	0.04	4.3
		2.54				
$CuY_{B'}$	B3LYP	1.98	B3LYP	0.59	0.03	3.3
		1.99				
$iCuY_B$	BP	2.00	BP	0.56	0.35	40.5
		2.02				
		2.24				
		2.64				
$iCuY_{B'}$	BP	1.94	BP	0.58	0.48	61.6
		1.95				
		1.99				
		2.00				
$iCuY_{B'}$	B3LYP	1.93	B3LYP	0.74	0.57	73.5
		1.94				
		1.97				
		1.99				
$iCuY_{B'}^{QM/MM}$	QM/MM	1.96	BP	0.73	0.42	47.9
		1.96				
		2.01				
		2.03				

[a] $Y_B = Si_2Al_2O_8H_8^{2-}$.

of the $d_{x^2-y^2}$ of Cu(II) with the p orbitals of the ring oxygen atoms. The stabilization is increased when this overlap involves four ring oxygen coordinated to the metal instead of only three. This overlap is larger for site II than for site III because Cu(II) lies in the ring plane. In the case of site III, the four ring oxygen atoms are outside the plane of the Si/Al ring and the Cu cation is itself on top of the oxygen atoms plane in a quasi-pyramidal environment for a better overlap with the O 2p orbitals.

TABLE 2: Site II Models, Cu−O Bond Lengths, Geometry Optimization Methods and Calculation Types, Mulliken Cu Net Charge, Spin Density, and A_{dip} Values (6-31G(d) for All Atoms and Wachters for Cu)

models[a]	geometry optimization method	d_{Cu-O} (Å)	calculation energy method	Mulliken metal net charge	spin density	A_{dip} (10^{-4} cm^{-1})
CuY_{F1}	B3LYP	2.01	B3LYP	0.79	0.65	79.8
		2.04	BP	0.63	0.51	61.3
		2.09				
		2.21				
$CuY_{F1'}$	B3LYP	1.94	B3LYP	0.79	0.62	74.4
		1.96	BP	0.64	0.50	59.0
		2.04				
		2.65				
$CuY_{F1'}$	BP	1.97	BP	0.63	0.48	55.7
		1.97				
		2.10				
		2.60				
CuY_{F2}	B3LYP	2.03	B3LYP	0.80	0.68	83.5
		2.03	BP	0.66	0.55	68.0
		2.08				
		2.09				
$CuY_{F1}^{QM/MM}$	QM/MM	2.06	BP	0.58	0.42	52.1
		2.12				
		2.13				
		2.14				
CuY_{F1}^{MM}	MM	2.12	B3LYP	0.74	0.52	63.0
		2.13	BP	0.62	0.44	50.2
		2.16				
		2.17				
CuY_{F1}^{MM} [b]	MM		B3LYP	0.69	0.54	64.5

[a] $Y_F = Si_4Al_2O_{18}H_{12}^{2-}$ [b] The OH terminations of the $Si_4Al_2O_{18}H_{12}^{2-}$ cluster are substituted with H leading to the $Si_4Al_2O_6H_{12}^{2-}$ cluster.

III. Results and Discussion

III-1. Models of Cu−Y: Charge and Spin Density on Cu-(II). A previous study[38] has shown that the size of the model, the Si/Al ratio, the sites, and the coordination of Cu do not induce a significant variation of the atomic charge on Cu for the different models (Figure 2). As a consequence, the smallest model, Y_B, can be used to represent Cu(II) in site III. The electronic structure analysis shows that the charge transferred from the zeolite to Cu fills substantially its 3d hole and contributes to some population of the 4s and 4p Cu orbitals.[38] Actually, this conclusion can be extended to all of the models reported in Tables 1 and 2, including the models for site II. The total charge on copper remains very close to 28, whatever the model is, showing a clear charge transfer (CT) of around $1e^-$ from the zeolite to the metal. This strong CT contributes also to decrease the spin density on Cu to much less than 1, whereas the isolated Cu^{2+} ion has a $3d^9$ electronic configuration. For all models, the spin density on Cu is characteristic of the 3d orbitals, with no contribution of the 4s and 4p subshells.

The analysis of the calculated spin density for all of the models investigated shows that, in contrast to the charge, this parameter is very dependent on the cluster. It does not specifically depends on the cluster size itself (Figure 2) but more on the number and lengths of the Cu−O bonds: the Cu spin density decreases when the Cu−O bond distances increase, that is, with decreasing Cu−O interactions. In fact, the metal character of the SOMO increases from a two- to a four-coordinated Cu, increasing its spin density from less than 0.1 up to 0.5−0.6. However, the number and lengths of the Cu−O bonds are not the only criteria for predicting Cu spin density: the calculated Cu spin densities in the $iCuY_{B'}$ and $CuY_{F1'}$ structures are comparable, whereas the first complex contains four short Cu−O and the second one only three short Cu−O

TABLE 3: Mulliken Cu Net Charge, Spin Density, SOMO (Energy), and Gross Population versus Calculation Methods (6-31G(d) for All Atoms and Wachters for Cu, except When Indicated)

$iCuY_{B'}$	SOMO−LUMO gap (eV)	charge on Cu	spin density on Cu	SOMO composition d Cu/p O ratio	Cu electronic configuration[a] 4s	4p	3d
BP	0.87	0.58	0.48	0.20	0.39	0.39	9.64
		0.52[b]	0.48[b]				
		1.10[c]	0.50[c]				
		0.56[d]	0.49[d]				
BLYP	0.87	0.56	0.48	0.17	0.40	0.40	9.64
B3LYP	3.09	0.71	0.57	0.06	0.35	0.37	9.57
		0.37[b]	0.57[b]				
		1.18[c]	0.60[c]				
		0.65[d]	0.57[d]				
B1LYP	3.77	0.74	0.60	0.06	0.35	0.37	9.54
UHF	11.48	1.21	0.88	0.03	0.26	0.29	9.24

[a] Gross atomic population. [b] A 6-311+G(2d,2p) extended basis set has been used on atoms with the Wachters basis set on Cu. [c] An IGLOIII extended basis set has been used on atoms with the Wachters basis set on Cu. [d] The OH terminations of the $Si_2Al_2O_{12}H_8^{2-}$ cluster are substituted with H leading to the $Si_2Al_2O_4H_8^{2-}$ cluster.

bonds. These results show thus how the validity of the cluster approach is related with a realistic description of the site geometry.

III-2. Influence of the Methodology on the Charge and Spin Densities. To analyze the effect of the method used (UHF, DFT, hybrid), we have chosen to compare the charge and spin densities of $iCuY_{B'}$ provided by these different methodologies. The results displayed in Table 3 show clearly the differences.

From GGA (BP) to HF, the net charge on copper is doubled whereas the gross atomic population analysis shows a decreased CT. At the same time, the spin density increases with an increasing contribution of HF exchange in the calculations. As expected, HF results correspond to a much less covalent metal−oxygen bonding than GGA-DFT, with intermediate results for hybrid schemes. Because the HF method favors ionic situations, the zeolite to metal CT is underestimated with respect to GGA, leading to a much larger spin density on Cu. The use of different basis sets for zeolite atoms has shown that the spin density is not very sensitive to the basis set extension, whereas the net charge on copper can vary very significantly with it, specially in the case of B3LYP calculations (from 0.71 using 6-31G(d) to 0.37 using 6-311+G(2d,2p) basis set for $iCuY_{B'}$ and to 1.18 using IGLOIII basis set (Table 3)).

H terminations, instead of OH's, lead to negligible changes of the spin density. For example, the Cu spin density estimated for $iCuY_{B'}$ with OH's is very comparable to that obtained with H's (Table 3). Similarly, H terminations in CuY_{F1}^{MM} are associated with a Cu spin density of 0.69, which is not significantly different from 0.74 when Si and Al are saturated with OH's (Table 2). Hence, we can say that we have shown that there is no effect of the size of the cluster chosen to represent the Cu sites (section III-1), that the way in which the dangling bonds are saturated does not significantly alter the main conclusions concerning the influence of the geometry (Cu−O bonds), and that the methodology (inclusion of HF exchange) is determinant for the calculated spin densities.

III-3. Calculated and Experimental Hyperfine Coupling Constants. *III-3-1. Experimental EPR Data.* To compare our calculations with experimental results, we have considered the measurements obtained from dehydrated Y zeolites with a Si/Al ratio close to 2.5.[4−6,9,11,12,39,40] Depending on the measurements, one, two, or three different signals are observed, resulting probably from differences in the preparation of the material,

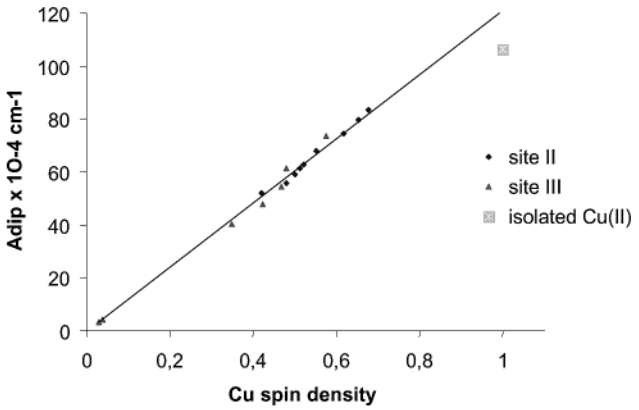

Figure 4. Calculated A_{dip} values as a function of the calculated Cu spin density. A_{dip} values are taken from Tables 1 and 2, except for models without QM optimization of the Cu position.

such as the proportion and nature of Cu(II) cocations, the Cu content, the Si/Al ratio, the temperature of synthesis, and the dehydration conditions. Experimental conditions are probably also responsible for the differences in the experimental g and A values. Two different groups of signals can be distinguished: the first one has a $g_{||}$ value of 2.32−2.35 associated with an $A_{||}$ hyperfine value in the range of (145.8−179) × 10^{-4} cm^{-1}; the second one has a higher $g_{||}$ value of 2.36−2.39 and a smaller $A_{||}$ hyperfine value in the range of (112.0−145) × 10^{-4} cm^{-1}; $g_{\perp}$ (2.06−2.07) and $A_{\perp}$ ((12.5−22) × 10^{-4} cm^{-1}) vary much less.

To compare with the hyperfine coupling constants calculated for our model clusters, "experimental" A_{dip} values have been deduced from the experimental $A_{||}$ and $A_{\perp}$ coupling constants. The A_{dip} range of values corresponding to the first group is 33.2−44.2, and the second one is 42.5−53.6. These "experimental" A_{dip} values can be compared with the calculated values reported in Tables 1 and 2. It is interesting to note that the variations of the experimental A values are quite large, showing the sensitivity of the hyperfine coupling to the local environment of the unpaired electron.

III-3-2. Comparison between "Experimental" and Calculated Hyperfine Coupling. The variation of the hyperfine coupling constant A_{dip} with respect to the spin density on Cu is illustrated in Figure 4, showing a linear variation going from the origin at zero to the d^9 Cu^{2+} ion.

According to the expression of the anisotropic coupling (section II-2), the linear relationship between A_{dip} and the spin density on Cu is due to a quasi-constant value of the $\langle r^{-3} \rangle$ integral, reflecting similar first-neighbor interactions. This relation is not affected by the size of the model cluster or by the methodology. Larger A_{dip} values are just related to larger spin densities. Because HF and hybrid methods lead to a larger localization of the unpaired electron on the metal, the A_{dip} values calculated from these methods are larger than those obtained from GGA. Using this linear relationship and "experimental" A_{dip} values obtained for Cu−Y zeolites, we can thus define the range of Cu spin densities that corresponds to the range of "experimental" A_{dip} values. As shown in Figure 4, the "experimental" Cu spin densities can be evaluated to vary between 0.3 and 0.45. Keeping in mind that second-order contributions to the anisotropic coupling constants would slightly decrease calculated values, we can draw several remarks from this comparison: the hyperfine couplings calculated with hybrid methods are too large for both sites II and sites III to fit with "experimental" A_{dip} values, leading to the conclusion that GGA estimates of the spin distribution between Cu and the zeolite

are more reasonable; bicoordinated Cu at site III quite unlikely corresponds to one observed EPR signal; calculated hyperfine coupling parameters are very sensitive to the structures and the A_{dip} values are generally larger for site II than for site III for the models containing Cu in ideal positions, although this trend cannot be considered as a rule; the hyperfine coupling constants for models cut from simulated solids (MM clusters) are in better agreement with the experimental values than those calculated for isolated optimized clusters (at least, at the level of approximation of our EPR calculations). Indeed, a geometry that takes into account the next shells of neighbors, in particular, the presence of the other extraframework cations, can lead to a different local framework around the Cu cation. In this respect, the orientation of the O atoms involved in the four- and six-membered rings can change significantly.

The spin density evaluated from the "experimental" A_{dip} hyperfine parameters is a good indication of the delocalization of the unpaired electron, which shares its time between the metal and the zeolite framework. This is an indication that the reactivity of Cu(II) zeolites should be understood as a supramolecular reactivity. In fact, the TM cation should be considered as associated with its framework but not as a divalent TM cation involved in an ion-pair system because such a representation does not take into account the redistribution of the electron density over the whole sytem.

In a previous work,[12] the authors proposed that the Al distribution in the site II six-membered ring (containing 1−3 Al), and not the site differences, governs the EPR signals. Indeed, they found that two different Cu−site II structures correspond to two different *g* values. According to our results, different geometries (three short/one long or four short Cu−O bonds) may exist at both sites II and III, but this difference is not sufficient to assign uniquely the experimental EPR signals.

Conclusion

In this work, we used the calculated anisotropic hyperfine coupling constants for models of sites II and III of a Cu(II)−Y zeolite to get insight into the electronic structures of these Cu sites. On the basis of a good correlation between A_{dip} values and the spin density on copper, whatever the methods are, GGA or B3LYP, we have shown that the hyperfine coupling is extremely sensitive to the geometry of the Cu(II) site. In fact, the hyperfine coupling decreases with decreasing the coordination number of Cu(II) or increasing the Cu(II)−O bond distances. However, a more detailed analysis of the results reveals that the count of Cu−O short and long bonds is not sufficient to rationalize the relationship between the site geometry and the experimental EPR signal. Despite the incertitude on the calculated hyperfine coupling constants, due to the incertitude on the real local geometries and to the neglect of second-order terms, our results show that both sites II and III are possible Cu locations. This study has also shown that, using model clusters and the linear relationship between the calculated hyperfine coupling constants and Cu spin densities, one can estimate the delocalization of the unpaired electron in Cu(II) zeolites.

Acknowledgment. These calculations were carried out on the IBM SP3 computer of the CINES (Centre Informatique National de l'Enseignement Supérieur) in Montpellier (France) and on the NEC-SX5 of the IDRIS (Institut des Ressources en Informatique Scientifique) in Orsay (France).

References and Notes

(1) Byrne, Y. W. Patent 4,961,917, 1990.
(2) Byrne, Y. W.; Chen, Y. M.; Speronello, B. K. *Catal. Today*. **1992**, *13*, 33.
(3) Descat, G.; Hamon, C. Patent 5,369,070, 1994.
(4) Liu, S.-B.; Lin, T.-S.; Yang, T−C.; Chen, T.-H.; Hong, E.-C.; Ryoo, R. *J. Phys. Chem.* **1995**, *99*, 8277.
(5) Schoonheydt, R. A. *Catal. Rev.—Sci. Eng.* **1993**, *35*, 129.
(6) Conesa, J. C.; Soria, J. *J. Chem. Soc., Faraday Trans.* **1979**, *75*, 406.
(7) Turkevitch, J.; Ono, Y.; Soria, J. *J. Catal.* **1972**, *25*, 44.
(8) Ichikawa, T.; Kevan, L. *J. Phys. Chem.* **1983**, *87*, 4433.
(9) Yu, J.-S.; Kevan, L. *J. Phys. Chem.* **1990**, *94*, 7612.
(10) Matar, K.; Goldfarb, D. *J. Phys. Chem.* **1992**, *96*, 3100.
(11) Levi, Z.; Matar, K.; Raitsimring, A. M.; Goldfarb, D. *Pure Appl. Chem.* **1992**, *64*, 799.
(12) Pierloot, K.; Delabie, A.; Groothaert, M. H.; Schoonheydt, R. A. *Phys. Chem. Chem. Phys.* **2001**, *3*, 2174.
(13) Maxwell, I. E.; de Boer, J. J. *J. Phys. Chem.* **1975**, *79*, 1874.
(14) Kieger, S.; Delahay, G.; Coq, B. *Appl. Catal. B* **2000**, *25*, 1.
(15) Kieger, S.; Delahay, G.; Coq, B.; Neveu, B. *J. Catal.* **1999**, *183*, 267.
(16) Jilinskaya, H.; Delahay, G. Personal communication.
(17) Casida, M. E.; Daul, C.; Goursot, A.; Koester, A.; Pettersson, L.; Proynov, E.; St-Amant, A.; Salahub, D. R.; Duarte, H.; Godbout, N.; Guan, J.; Jamorski, C.; Leboeuf, M.; Malkin, V.; Malkina, O.; Sim, F.; Vela, A. *deMon*, version KS3; 1996.
(18) Frisch, M. J.; Trucks, G. W.; Schlegel, H. B.; Scuseria, G. E.; Robb, M. A.; Cheeseman, J. R.; Zakrzewski, V. G.; Montgomery, J. A., Jr.; Stratmann, R. E.; Burant, J. C.; Dapprich, S.; Millam, J. M.; Daniels, A. D.; Kudin, K. N.; Strain, M. C.; Farkas, O.; Tomasi, J.; Barone, V.; Cossi, M.; Cammi, R.; Mennucci, B.; Pomelli, C.; Adamo, C.; Clifford, S.; Ochterski, J.; Petersson, G. A.; Ayala, P. Y.; Cui, Q.; Morokuma, K.; Malick, D. K.; Rabuck, A. D.; Raghavachari, K.; Foresman, J. B.; Cioslowski, J.; Ortiz, J. V.; Stefanov, B. B.; Liu, G.; Liashenko, A.; Piskorz, P.; Komaromi, I.; Gomperts, R.; Martin, R. L.; Fox, D. J.; Keith, T.; Al-Laham, M. A.; Peng, C. Y.; Nanayakkara, A.; Gonzalez, C.; Challacombe, M.; Gill, P. M. W.; Johnson, B. G.; Chen, W.; Wong, M. W.; Andres, J. L.; Head-Gordon, M.; Replogle, E. S.; Pople, J. A. *Gaussian 98*, revision A.9; Gaussian, Inc.: Pittsburgh, PA, 1998.
(19) Flükiger, P.; Lüthi, H.-P.; Portmann, S.; Weber, J. *MOLEKEL*, revision 4.1; Swiss Center for Scientific Computing: Manno, Switzerland, 2000−2001.
(20) Vosko, S. H.; Wilk, L.; Nusair, M. *Can. J. Phys.* **1980**, *58*, 1200.
(21) Perdew, J. P.; Chevary, J. A.; Vosko, S. H.; Jackson, K. A.; Pederson, M. R.; Singh, D.; Fiolhais, C. *Phys. Rev. B* **1992**, *46*, 6671.
(22) Becke, A. D. *Phys. Rev. A* **1988**, *38*, 3098.
(23) Perdew, J. P. *Phys. Rev. B* **1986**, *33*, 8822.
(24) Lee, C.; Yang, W.; Parr, R. G. *Phys. Rev. B* **1988**, *37*, 785.
(25) Becke, A. D. *J. Chem. Phys.* **1993**, *98*, 5648.
(26) Wachters, A. J. H. *J. Chem. Phys.* **1970**, *52*, 1033.
(27) Godbout, N.; Salahub, D. R.; Andzelm, J.; Wimmer, E. *Can. J. Chem.* **1992**, *70*, 560.
(28) Hariharan, P. C.; Pople, J. A. *Theor. Chim. Acta* **1973**, *28*, 213.
(29) Francl, M. M.; Petro, W. J.; Hehre, W. J.; Binkley, J. S.; Gordon, M. S.; DeFre, D. J.; Pople, J. A. *J. Chem. Phys.* **1982**, *77*, 3654.
(30) Krishnan, R.; Binkley, J. S.; Seeger, R.; Pople, J. A. *J. Chem. Phys.* **1980**, *72*, 650.
(31) Clark, T.; Chandrasekhar, J.; Schleyer, P. v. R. *J. Comput. Chem.* **1983**, *4*, 294.
(32) Kutzelnigg, W.; Fleischer, U.; Schindler, M. *NMR−Basic Principles and Progress*; Springer-Verlag: Heidelberg, Germany, 1990; Vol. 23165.
(33) Munzarova, M.; Kaupp, M. *J. Phys. Chem. A* **1999**, *103*, 9966.
(34) Malkin, V. G.; Malkina, O. L.; Eriksson, L. A.; Salahub, D. R. In *A Tool for Chemistry*; Politzer, P., Seminario, J., Eds.; Elsevier: Amsterdam, 1995; Vol. 2.
(35) Mabbs, F. E.; Collison, D. *Electron Paramagnetic Resonance of d Transition Metal Compounds*; Elsevier: Amsterdam, 1992.
(36) *Cerius2. Molecular modeling software for materials research, Accelrys*; Biosym Technologies: San Diego, CA, 1993.
(37) Dedecek, J.; Wichterlova, B. *J. Phys. Chem. B* **1997**, *101*, 10233.
(38) Berthomieu, D.; Krishnamurty, S.; Coq, B.; Delahay, G.; Goursot, A. *J. Phys. Chem. B* **2001**, *105*, 1149.
(39) Nacache, C.; Ben Taarit, Y. *Chem. Phys. Lett.* **1971**, *11*, 11.
(40) Carl, P. J.; Larsen, S. C. *J. Phys. Chem. B* **2000**, *104*, 6568.